T.C. BIOLOGICAL AND BIOMIMETIC MATERIALS

^{1}H NMR spectroscopy study of structural water in rehydrated biocomposite of *Spongilla lacustris* freshwater demosponge origin

Tatiana Krupska[1] · Marcin Wysokowski[2,3] · Iaroslav Petrenko[3] · Yuliya Khrunyk[4,5] · Krzysztof Nowacki[6] · Hermann Ehrlich[3,7] · Vladimir V. Turov[1]

Abstract

Biocomposites of sponge origin attract scientific attention due to their renewability as well as special properties. Dried skeletons of fresh water demosponge *Spongilla lacustris* represent unique kind of naturally occurring silica-chitin-based biocomposites with long history of their applications in dermatocosmetics. However, there is still a lack of knowledge on their physico-chemical properties in model systems. The aim of this work was to model drug systems based on *S. lacustris* powdered biocomposite, water and a hydrophobic medium, which served as an analog of an oil base. Both thermogravimetric analysis and ^{1}H NMR spectroscopy study of structural water in rehydrated biocomposite lead to obtaining of interesting experimental data useful for preparation of biocosmetic products.

Keywords *Spongilla lacustris* · Bio-silica · ^{1}H NMR · Biocosmetics

✉ Marcin Wysokowski
marcin.wysokowski@put.poznan.pl

Vladimir V. Turov
v_turov@ukr.net

1   Chuiko Institute of Surface Chemistry of the NAS of Ukraine, General Naumov Str. 17, Kiev 03164, Ukraine

2   Faculty of Chemical Technology, Institute of Chemical Technology and Engineering, Poznan University of Technology, Berdychowo 4, 60965 Poznan, Poland

3   Institute of Electronics and Sensor Materials, TU Bergakademie Freiberg, Gustav-Zeuner str. 3, 09599 Freiberg, Germany

4   Ural Federal University, Mira Str. 19, 620002 Ekaterinburg, Russia

5   The Institute of High Temperature Electrochemistry of the Ural Branch of the Russian Academy of Sciences, Akademicheskaya Str. 20, 620990 Ekaterinburg, Russia

6   Institute of Chemistry and Technical Electrochemistry, Poznan University of Technology, ul. Berdychowo 4, 60-965 Poznan, Poland

7   Center for Advanced Technology, Adam Mickiewicz University, 61614 Poznan, Poland

1 Introduction

Sponges (Porifera) represent an ancient and unique phylum of the first multicellular organisms to have inhabited our planet. They have survived since Precambrian due to the ability to synthetize a broad diversity of secondary metabolites with cytotoxic and antibiotic-like activities as well as the formation of robust skeletal structures made of biosilica and calcium carbonates (see for review [1, 2]). Siliceous spicules remain to be one of the typical skeletal formations found in diverse sponges, which belong to the Demospongiae class. They function as mechanical support for organic matrix as well as due to very sharp apical ends can protect the sponge body from predators (i.e., fish, turtles, etc.). Intriguingly, the presence of sharp up to 300 µm-long spicules contributed to the use of fresh water sponges such as *Spongilla lacustris* in the traditional and folk medicine in China, Russia, Ukraine and Thailand [3, 4]. In contrast to biomimetically designed diverse silica-collagen [5–11] and silica-chitin composites [12–16] of sponges origin, dried skeletons of *S. lacustris* represent unique source of naturally occurring biocomposites with high potential for applications in dermatocosmetics. In recent years, dried *S. lacustris* powdered biocomposites has been widely applied as a component for masks in the treatment of such cosmetic skin imperfections as acne, pigmentation after sunburn, bruising and other skin conditions [17–21]

Fig. 1 Microphotographs of *S. lacustris* powder (**a**, **b**) as example of naturally occurring biocomposite. Biosilica-based sharp spicules are tightly bound into chitinous matrix
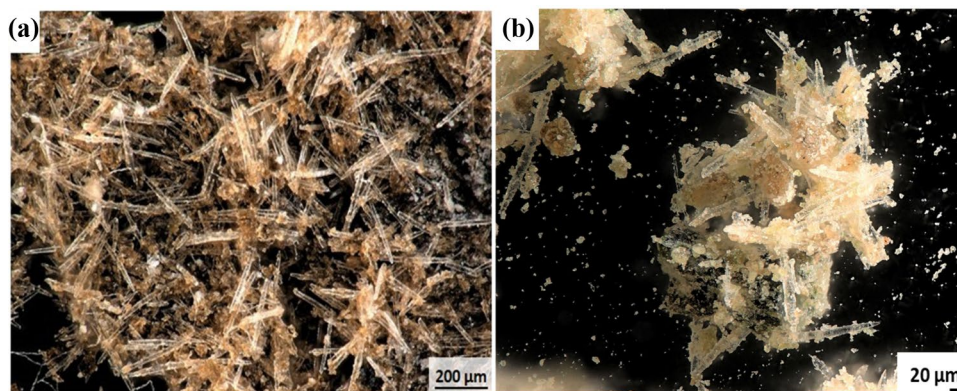
including cellulite [22]. Such biocomposite contains organic residues (chitin, microalgae) [23, 24]) and biosilica-based spicules (Fig. 1). The presence of sharp spicules in corresponding dermatocosmetic products enhances the penetration of drugs and other substances through the skin [20, 21, 25]. The unique advantages of transdermal drug delivery over the other routes of drug administration include delayed release drug delivery and controlled drug release rate [26–28]. Notably, the use of cosmetic masks in the form of both aqueous and oily suspensions is recommended.

The effectiveness of dosage forms based on biological products depends on the bioavailability of active substances desorbed from the natural component of the composite into an aqueous or aqueous-organic medium serving as the liquid base of the composite (dispersion medium). Subsequently, these substances come into contact with the skin or mucous membranes and are absorbed by the body. The main parameter determining the retention time of solution components in the adsorption layer, composed of solid particles of biomaterials origin, can be the surface energy of solid-water system, which is connected with the total decrease in water free energy due to the presence of a phase boundary (adsorption interactions). Surface energy can be analyzed using the data of wetting warmth [29] and low-temperature ^{1}H NMR spectroscopy, the latter is based on the study of the effect of solid–liquid interphase interactions on the temperature of water–ice phase transition [30–33].

The aim of this work was for the first time to model drug systems based on *S. lacustris* powdered biocomposite, water and a hydrophobic medium, which served as an analog of an oil base. The analyses were conducted employing low-temperature ^{1}H NMR spectroscopy [30–32], which evaluates an average number of hydrogen bonds involving each water molecule (based on the value of chemical shift of adsorbed water), as well as the radius of adsorbed water clusters and the change of Gibbs free energy of water in adsorbed layers taking into account the data on the depression of freezing temperature.

2 Materials and methods

Biocomposite of *Spongilla lacustris* freshwater demosponge (Fig. 1) has been purchased from Farmakom Ltd (Kharkiv, Ukraine). It is officially used for cosmetic applications according to ISO 9001 and ISO 22000.

2.1 ^{1}H NMR spectroscopy

^{1}H NMR spectra were recorded in air, deuterochloroform and deuterochloroform/deuterotrifluoroacetic acid (TFAA). Deuterium substances were used to avoid the presence of extraneous intense signals in the spectra. ^{1}H NMR spectra were recorded using a high-resolution NMR spectrometer (Varian "Mercury") at an operating frequency of 400 MHz. The conventional spectra were recorded with a proton 90° pulse length of 3.0 µs and the spectral width of 20 kHz.

1H NMR spectra of static samples (volume of ∼ 0.5 cm^3 placed into a 5 mm ampoule) of *S. lacustris* in air, chloroform-d or TFAA media were recorded using Varian 400 Mercury spectrometer employing 60° pulses of 3 µs duration. Temperature control (Bruker VT-1000) was accurate and precise to within ± 1 K. To prevent supercooling, the spectra were recorded starting at $T = 200$–210 K; samples were precooled to this temperature at a cooling rate of 5 K/min. Next, samples were heated up to 280–285 K. Such conditions provided an equilibrium state of samples at each temperature.

Signal intensities were detected by measuring the area of peaks by the means of the procedure of decomposing the signal into its components under the Gaussian line shape assumption, as well as by optimizing the zero line and phase with an accuracy of no less than 5% for well-resolved signals. To prevent supercooling of water in studied objects, the non-freezing water concentrations were recorded in heated samples, which were previously cooled to a temperature of 210 K. The method of NMR measurements, the analysis of thermodynamic characteristics and

the calculation of the radius of interphase water clusters are described in detail in [30–33].

To determine the geometric dimensions of the clusters of adsorbed water, the Gibbs–Thomson equation was used, relating the radius of a spherical or cylindrical water cluster or domain (R) to the value of the freezing point depression [34, 35]:

$$\Delta T_m = T_m(R) - T_{m,\infty} = \frac{2\sigma_{sl}T_{m,\infty}}{\Delta H_f \rho R}, \tag{1}$$

where $T_m(R)$ is the melting temperature of ice localized in pores of radius R, $T_{m,\infty}$ is the melting point of bulk ice, ρ is the density of the solid phase, σ_{sl} is the interaction energy between a solid surface and liquid, and ΔH_f is the volume enthalpy of melting.

The process of freezing (melting) of interphase water localized within solid porous matrix corresponds to the changes in Gibbs free energy, caused by the effects of limited space and the natural interface of the phases. The difference from the bulk process lessens inversely to the distance of water layer from the surface. The water that freezes at $T = 273$ K has properties, which correspond to bulk water, and as the temperature decreases (without taking into account the supercooling effect), the layers of water that are closer to the surface start freezing. Changes in the free energy of bound water (ice) follow the ratio:

$$\Delta G_{ice} = -0.036(273.15 - T), \tag{2}$$

where the numerical coefficient is a parameter related to the temperature coefficient of the Gibbs free energy variation for ice [36]. While determining the temperature dependence of the unfrozen water concentration $C_{uw}(T)$ based on the value of signal intensity in accordance with the procedure detailed in [30–33], the amount of strongly and weakly bonded water and the thermodynamic characteristics of these layers can be calculated.

The water interphase energy at the boundary with solid particles or in its aqueous solutions was determined as the modulus of the total decrease in the free energy of water due to the presence of phase interface [30–33] according to the formula:

$$\gamma_S = -K \int_{0}^{C_{uw}^{max}} \Delta G(C_{uw}) dC_{uw}, \tag{3}$$

where C_{uw}^{max} is total amount of non-freezing water at $T = 273$ K.

The magnitude of interfacial energy is a convenient parameter to compare the binding energy of water in different systems, especially if the amount of water in them is the same.

Samples were observed using advanced imaging and measurement system consisting of Keyence VHX-6000 digital optical microscope and the swing-head zoom lenses VH-Z20R (magnification up to 200 ×) and VH-Z100UR (magnification up to 1000 ×). *S. lacustris* powder (Fig. 1) has been provided by Farmakom Ltd (Kharkiv, Ukraine).

3 Results and discussion

Microphotographs of *S. lacustris* biocomposite powder are represented in Fig. 1. Siliceous spicules are clearly visible in digital stereo microscopy images.

The thermogravimetric analysis data of the rehydrated *S. lacustris* sample, which was kept at 293 K for 24 h, are shown in Fig. 2. On the mass loss curve (TG curve) three main sections corresponding to the minima on the DTG curve can be distinguished. The first section within the region of $T < 150$ °C should be attributed to the removal of water, the amount of which is 430 mg per 1 g of dry matter. The second section indicates mass loss (150 °C $< T <$ 400 °C), which is caused by the destruction of the organic component of biological product, whereas the third section (400 °C $< T <$ 650 °C) is formed due to carbonization and CO_2 formation. The ash content of the sample accounts for 36% of its initial mass, which is due to a high amount of silica being a part of *S. lacustris* sample. Small endothermic as well as exothermic maxima correspond to water removal on the DTA curve and to the rest of the processes, respectively.

Figure 3 shows the spectra of *S. lacustris* samples recorded at different ^{1}H NMR temperatures, containing $C_{H_2O} = 430$ and 890 mg/g water in air (a, b), $CDCl_3$ medium (c, d) and chloroform medium with the addition of
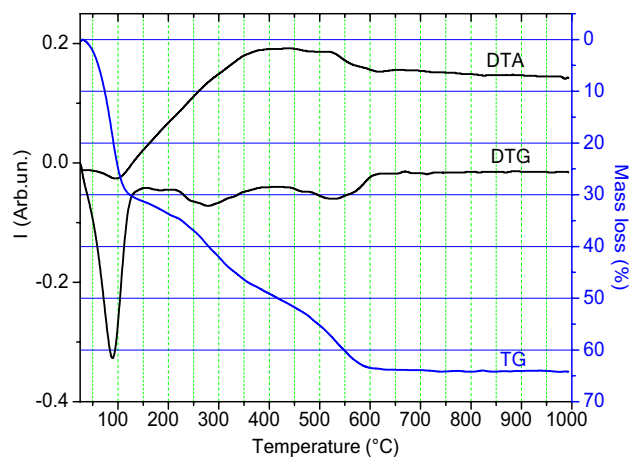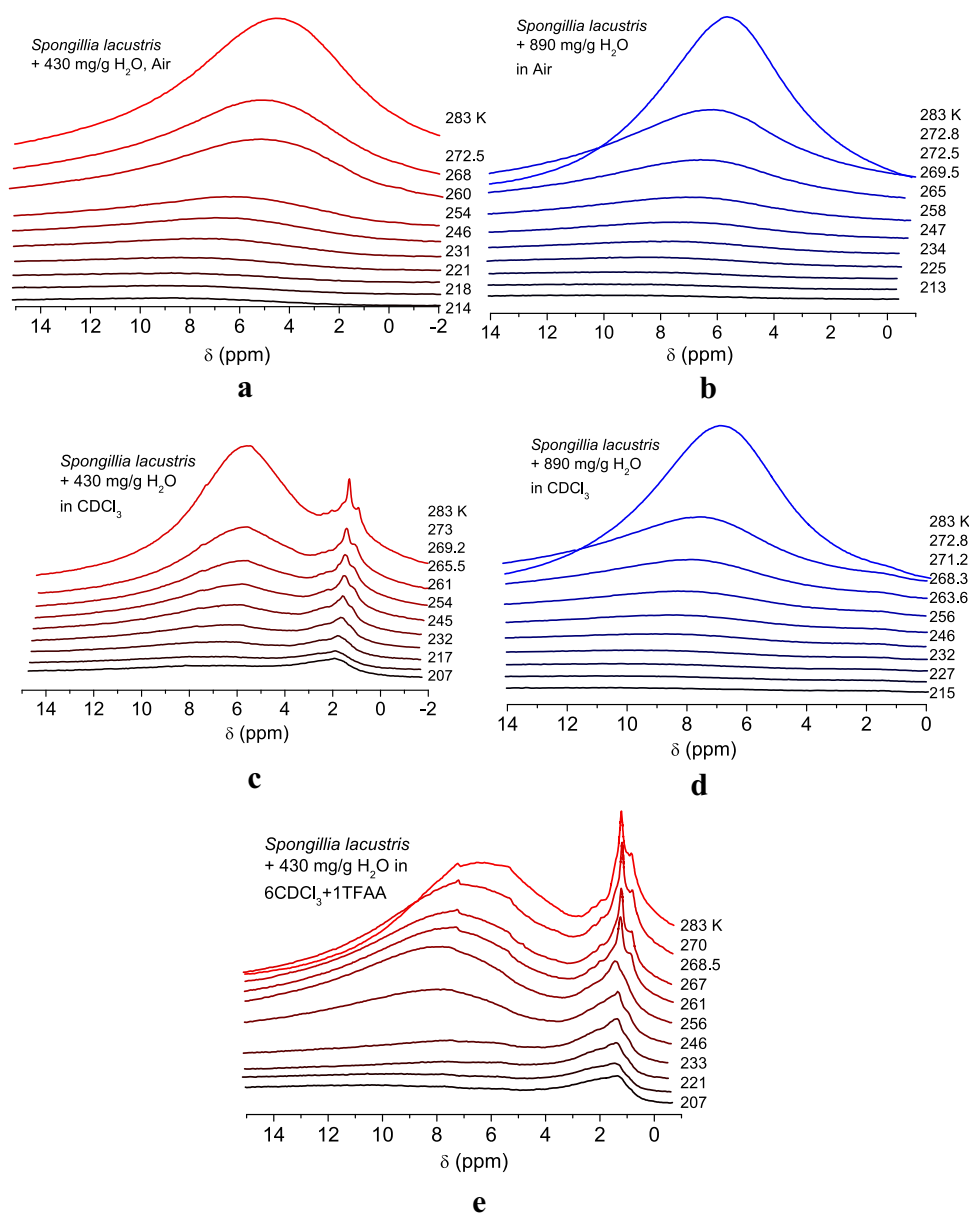

Fig. 2 Thermograms of the rehydrated *S. lacustris* powdered biocomposite

Fig. 3 The ^{1}H NMR spectra of *S. lacustris* biocomposite samples taken at different temperatures, containing $C_{H_2O} = 430$ and 890 mg/g of water in air (**a**, **b**), CDCl$_3$ (**c**, **d**) and 6 CDCl$_3$ + 1 TFAA (**e**)

deuterotrifluoroacetic acid (e). In air, one wide water signal is recorded in the spectra, the intensity of which decreases with temperature reduction due to partial freezing of interphase water, whereas the chemical shift is shifted to the region of large values reaching $\delta_H = 8$ ppm at $T = 214$ K (Fig. 3a). Since the increase in the ordering of the network of hydrogen bonds, caused by the formation of ice-like structures, increases the chemical shift to $\delta_H = 7$ ppm. [30–33], large values of the chemical shift should be attributed to an increase in the contribution of the acid group protons of *S. lacustris*.

In CDCl$_3$, the shape of the spectra changes. At $C_{H_2O} = 430$ mg/g (Fig. 3c), a group of intense signals appears with chemical shifts in the region $\delta_H = 1.5$-3 ppm. In this spectral region, one can expect the appearance of signals

of weakly associated (forming little hydrogen bonds with other molecules) water, as well as aliphatic protons of phospholipid groups that make up the cellular material. In view of the complex nature of the spectrum, it should be noted that for the *S. lacustris* sample this type of proton is the main one. Since cell membranes predominantly consist of phospholipids, it can be assumed that, at a selected level of hydration, chloroform easily penetrates the tissue of biological material of *S. lacustris* and dissolves in the membranes, increasing the mobility of phospholipid molecules. This effect increases with the inclusion of TFAA in the dispersion medium (Fig. 3e) and decreases with an increase in interstitial water concentration (Fig. 3d). It is likely that the high level of hydration of the biomaterial prevents direct

contact of hydrophobic medium with cells, thus reducing the possibility of its dissolution in cell membranes structures.

Taking into account the knowledge of the total amount of water in the samples prior to freezing, the concentrations of non-freezing water (C_{uw}) can be calculated based on the temperature dependences of the intensity of water NMR signal for each temperature and, using the data on C_{uw} and the formula (2), the values of Gibbs free energy change in the adsorbed water layer (ΔG) can be obtained. For the studied systems, the dependences $C_{uw}(T)$ and $\Delta G(C_{uw})$ are shown in Fig. 4.

The horizontal line in Fig. 4b allows us to divide interfacial water into strongly and weakly bound water (SBW and WBW, respectively). In this case, the fraction of water that freezes at $T < 265$ K ($\Delta G < -0.5$) [30–33] is considered to be strongly bound. According to the data in Fig. 4b, in both air and hydrophobic media, the amount of strongly bound water decreases with elevated hydration of the sample, but increases in the presence of TFAA. The diagram indicating the change in the magnitude of the interfacial energy (solid–water) calculated according to formula (3) based on the dependences (see Fig. 4b) is shown in Fig. 5d, whereas Fig. 5a–c demonstrate the radial distributions of interphase water clusters calculated by the Gibbs–Thomson formula (1). As expected, an increase in the amount of water in the sample led to the appearance of large interfacial water clusters (Fig. 5a, b). However, in this case, not an increase, but a reduction in interfacial energy of water (Fig. 5d) is observed, i.e., the total energy of water binding in the biomaterial decreases with elevated hydration of tissue. Perhaps this is due to the complex nature of changes in the distribution of water in the biomaterial depending on the level of its rehydration. For example, it can be suggested that intracellular water is more strongly bound than in the intercellular

space, but for its penetration into the cells, a certain amount of weakly bound water must be present within the intercellular space. At $C_{H_2O} = 430$ mg/g, a significant fraction of water does not penetrate the cells, being localized outside, where it is weaker bound to the surface of *S. lacustris* sample. The binding of water in the *S. lacustris* sample increases in weakly polar medium, especially at a low level of rehydration (Fig. 5b, d). This is due to a decrease in the average radius of the clusters of adsorbed water. The addition of a strong acid to the dispersion medium leads to a significant increase in the interfacial energy of water (Fig. 5d), caused by solvation effects. In the solution, acid molecules are hydrated and in order to reach their crystallization at low temperatures in the form of hexagonal ice it is necessary to expend energy equal to the energy of solvation. Moreover, most of the water freezes in the form of clusters with $R = 3$ nm (Fig. 5c).

The temperature dependences of the chemical shift for *S. lacustris* samples at different hydration in air and organic media are shown in Fig. 6. The values of the chemical shift turned out to be very large, especially at low temperatures, when most of the water freezes. In some cases, a chemical shift of water was recorded even to be higher than in the sample with the addition of TFAA. Therefore, on the surface of the dried *S. lacustris* biomaterial, there was a significant amount of acid groups with which water molecules were able to form hydrogen-bound complexes, and their dissociation into water led to a significant increase in the chemical shift of interfacial water.

In contrast to *S. lacustris* powder used in this study, recently discovered chitin-spicule composite material extracted from *Ochridaspongia rotunda* fresh water sponge [37] open the way to development of new ready to use surface-active cosmetic masks.
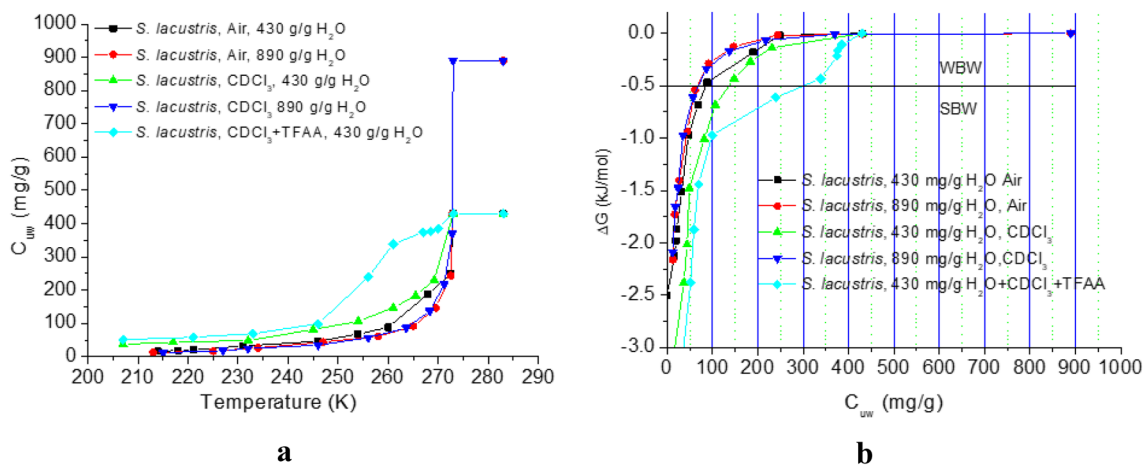

Fig. 4 Temperature dependences of the concentration of non-freezing water (**a**) and the dependences of the change in Gibbs free energy on the concentration of non-freezing water for *S. lacustris* biocomposite samples that differ in the amount of water in different media (**b**)

Fig. 5 The distribution of radii of interphase water clusters in *S. lacustris* biocomposite samples differing in water content and dispersion medium (**a–c**), and the diagram indicating changes in interphase energy (**d**)
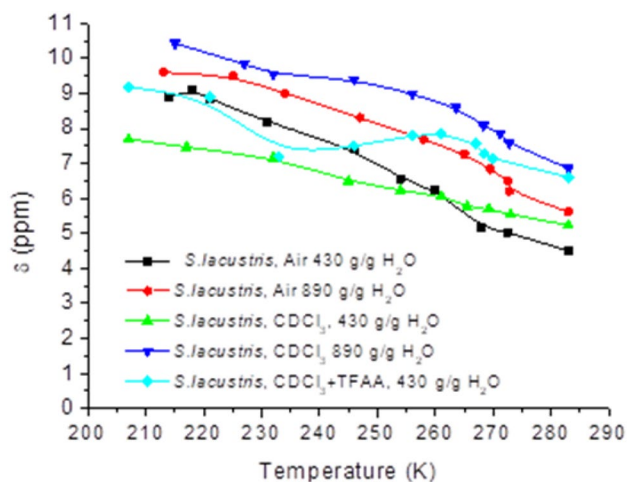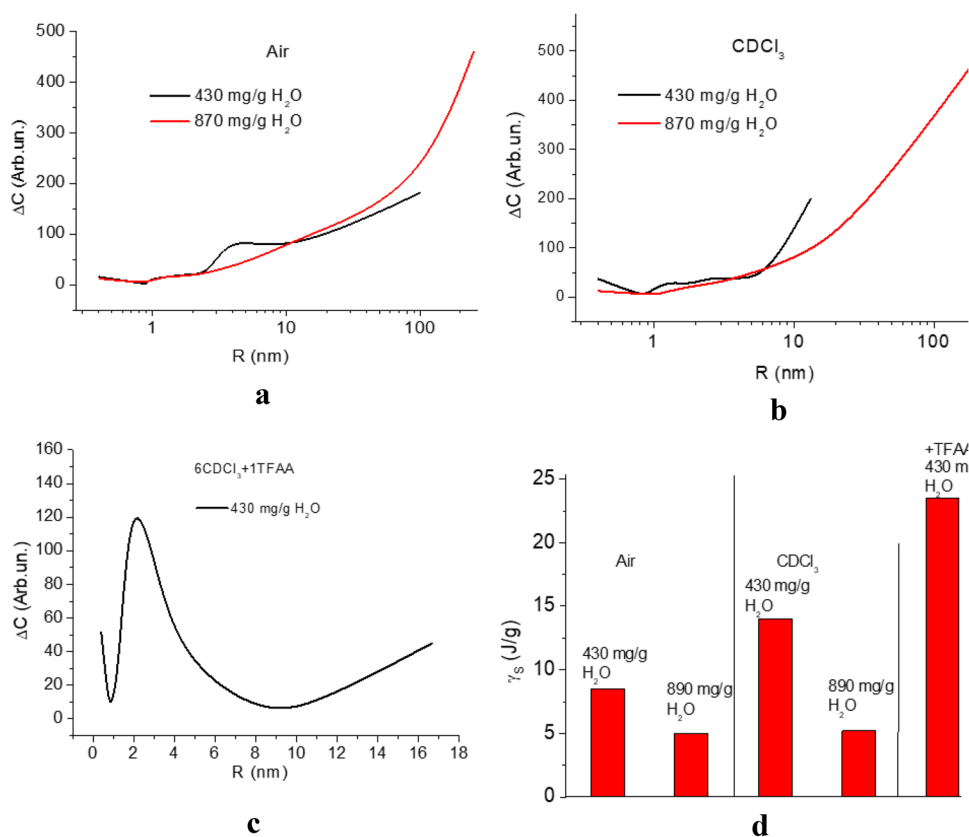

Fig. 6 Temperature dependences of the chemical shift for *S. lacustris* biocomposite samples with different hydration in air and organic media studied

here that the binding of water in *S. lacustris* biocomposite obtained by drying depends on the level of rehydration. It turned out that at $C_{H_2O} = 430$ mg/g, water binding is less than at $C_{H_2O} = 890$ mg/g, which may be due to the complex process of water penetration into partially dehydrated cellular material. A hydrophobic organic medium easily penetrates cell membranes at $C_{H_2O} = 430$ mg/g, but much less at $C_{H_2O} = 890$ mg/g. This phenomenon can be used for calculations of corresponding cosmetic creams, especially that which should be developed as anti-acne composites. The hydrophobic phase can be enriched with corresponding fat-soluble anti-inflammatory as well as anti-pain compounds, which are necessary to decrease possible irritation of skin surfaces due to spicule determined damage of the cellular membranes.

The magnitude of the chemical shift of water, associated with the tissues of rehydrated *S. lacustris*, approaches the values characteristic of strong acids, which indicates that a significant amount of acid groups capable of dissociation into a limited amount of water is present within the biocomposite.

4 Conclusions

Specific behavior of water/oil interphases within naturally occurring composites is of crucial interest for preparation of cosmetic products. It was shown for the first time

References

1. H. Ehrlich, Int. Geol. Rev. **52**, 661–699 (2010)
2. M. Wysokowski, T. Jesionowski, H. Ehrlich, Am. Mineral. **103**, 665–691 (2018)
3. K. Schroeder, Umsch Wiss Tech. **46**, 507–509 (1942)
4. M. Udompataikul, M. Wongniraspai, U. Showpittapornchai, A. Jariyapongsakul, J. Med. Assoc. Thai. **95**, S15–S20 (2012)
5. S. Heinemann, C. Knieb, H. Ehrlich, M. Meyer, H. Baltzer, H. Worch, T. Hanke, Adv. Eng. Mater. **9**(12), 1061–1068 (2007)
6. S. Heinemann, H. Ehrlich, C. Knieb, T. Hanke, Int. J. Mater. Res. **98**, 603–608 (2007)
7. H. Ehrlich et al., J Nanomater. **2008**, 623838 (2008)
8. H. Ehrlich et al., Chem. Mater. **22**(4), 1462–1471 (2010)
9. H. Ehrlich, K. Demadis, O. Pokrovsky, P. Koutsoukos, Chem. Rev. **110**, 4656–4689 (2010)
10. H. Ehrlich et al., Nat. Chem. **2**, 1084–1088 (2010)
11. H. Ehrlich, M. Wysokowski, S. Żółtowska-Aksamitowska, I. Petrenko, T. Jesionowski, Mar. Drugs **16**, 79 (2018)
12. H. Ehrlich et al., Adv. Opt. Mater. **4**, 1608–1613 (2016)
13. E. Steck, M. Burkhardt, H. Ehrlich, W. Richter, Xenotransplantation **17**, 153–159 (2010)
14. K. Spinde, M. Kammer, K. Freyer, H. Ehrlich, J. Vournakis, E. Brunner, Chem. Mater. **23**, 2973–2978 (2011)
15. M. Wysokowski et al., Mat. Sci. Eng. C **33**, 3935–3941 (2013)
16. M. Wysokowski et al., Int. J. Biol. Macromol. **78**, 224–229 (2015)
17. E. Yu, Patent RU 92002671A (1995)
18. M. Villani, Patent EP1663104B1 (2003)
19. M. Villani, Patent US7604821 B2 (2009)
20. M. Villani, Patent US8383100 B2 (2013)
21. M. Villani, Patent JP2010126310A (2010)
22. Z. Caihua et al. Patent CN106214535A (2016)
23. H. Ehrlich et al., J. Struct. Biol. **183**, 474–483 (2013)
24. H. Ehrlich et al., Proc. R Soc B **280**, 20130339 (2013)
25. I.V. Anchevsky, M.V. Glinskaya Patent RU2183967C1 (2001)
26. W. Dexiang, C. Ming, Patent CN105858669A (2016)
27. C. Ming, W. Dexiang, Patent CN105999535A (2016)
28. K, Tae-Gon, Patent WO2015156455A1 (2015)
29. Y.I. Tarasevich, Theor. Exp. Chem. **42**(3), 133–149 (2006)
30. V.M. Gunko, V.V. Turov, P.P. Gorbik, *The Water at the Interface* (Naukova Dumka, Kiev, 2009)
31. V.V. Turov, V.M. Gunko, *Clustered water and ways of its use* (Naukova Dumka, Kiev, 2011)
32. V.M. Gun'ko, V.V. Turov, *Nuclear Magnetic Resonance Studies of Interfacial Phenomena* (Taylor & Francis, New York, 2013)
33. V.M. Gun'ko et al., Adv Colloid Interface Sci **118**, 125–172 (2005)
34. D.W. Aksnes, K. Forl, L. Kimtys, Phys. Chem. Chem. Phys. **3**, 3203–3207 (2001)
35. O.V. Petrov, I. Furó, Prog. Nucl. Mag. Res. Spectrosc. **54**, 97–122 (2009)
36. V.P. Glushko, *Thermodynamic properties of individual substances* (Nauka, Moscow, 1978)
37. T. Talevski et al., Int. J. Biol. Macromol. **162**, 1187–1194 (2020)